Quantifying myelin density in the feline auditory cortex

Austin Robertson[1], Daniel J. Miller[2†], Adam Hull[3], Blake E. Butler[2,4,5*]

[1]Graduate program in Neuroscience, University of Western Ontario, London, ON, Canada
[2]Department of Psychology, University of Western Ontario, London, ON, Canada
[3]Undergraduate program in Neuroscience, University of Western Ontario, London, ON, Canada
[4]Western Institute for Neuroscience, University of Western Ontario, London, ON, Canada
[5]National Centre for Audiology, University of Western Ontario, London, ON, Canada

[†]Current address: Department of Evolution, Ecology, and Behavior, University of Illinois Urbana-Champagne, Urbana, IL, USA

[*]Correspondence should be addressed to:
Blake E. Butler, PhD
Department of Psychology
University of Western Ontario
1151 Richmond Street N.
London, ON
N6A5C1 Canada
bbutler9@uwo.ca

Blake E. Butler ORCID: 0000-0001-5287-3450
Daniel J. Miller ORCID: 0000-0002-4844-0828

Acknowledgements: The authors extend thanks to Katelyn Kittel for animal care support, and to Dr. Faraj Haddad for support with protocol development.

Abstract

The cerebral cortex comprises many distinct regions that differ in structure, function, and patterns of connectivity. Current approaches to parcellating these regions often take advantage of functional neuroimaging approaches that can identify regions involved in a particular process with reasonable spatial resolution. However neuroanatomical biomarkers are also very useful in identifying distinct cortical regions either in addition to, or in place of functional measures. For example, differences in myelin density are thought to relate to functional differences between regions, are sensitive to individual patterns of experience, and have been shown to vary across functional hierarchies in a predictable manner. Accordingly, the current study provides quantitative stereological estimates of myelin density for each of the 13 regions that make up the feline auditory cortex. We demonstrate that significant differences can be observed between auditory cortical regions, with the highest myelin density observed in the regions that comprise the auditory core (i.e., the primary auditory cortex and anterior auditory field). Moreover, our myeloarchitectonic map suggests that myelin density varies in a hierarchical fashion that conforms to the traditional model of spatial organization in auditory cortex. Taken together, these results establish myelin as a useful biomarker for parcellating auditory cortical regions, and provide detailed estimates against which other, less invasive methods of quantifying cortical myelination may be compared.

Keywords: Myelin, Auditory Cortex, Stereology, Feline

Introduction

Neuroscience has a longstanding interest in the relationships between the structure and functions of brain regions. Understanding the networks of areas that underlie complex behaviours is a common aim of cognitive neuroscientists, while identifying the underlying source of aberrant neural activity and/or behaviours is critical to neurological assessment and treatment. It is reasonable to propose that functionally distinct regions could be parcellated based on anatomical differences that reflect unique computational demands and patterns of connectivity to other brain areas. Accordingly, at the turn of the twentieth century at the direction of Oskar and Cecile Vogt, Brodmann published 'Localization in the Cerebral Cortex', in which he suggested that the brain could be divided into 52 areas based on differences in cytoarchitecture (Brodmann 1909). Impressively, this classic text provides many of the core principles that continue to guide attempts to resolve associations between cortical anatomy and function today (Annese 2009; Zilles 2018). For example, Brodmann's delineations form the basis of at least one probabilistic map used in modern imaging analyses (e.g., the Talirach atlas), while his description of a universal 6-layer structure in the cerebral cortex is now universally accepted (Zilles 2018). Early *functional* maps of the cerebral cortex expanded upon anatomical parcellations, relying on lesion and/or neurosurgical studies from small numbers of patients; however technological advances including functional magnetic resonance imaging (fMRI), transcranial magnetic stimulation (TMS), and transcranial direct current stimulation (tDCS) have dramatically accelerated their development. For example, fMRI has been used to dissociate regions that encode basic stimulus features (e.g., line fragments or particular orientations) from those that encode feature conjunctions and object representations in the visual cortical hierarchy (see Tootell et al. 1998 for review).

fMRI-based parcellation typically involves collecting a pair of fMRI image series that, when contrasted, reveal the pattern of neural activity evoked by a stimulus feature of interest (e.g., the pattern of activity evoked by a stationary dot is subtracted from the activity evoked by that same dot when in motion to reveal motion-sensitive areas of the brain). While this approach is widespread, it has inherent limitations. Firstly, it has been pointed out that the distribution of activity over the voxels within a region of interest may vary considerably depending on the context in which stimuli are presented, and the nature of the contrasts drawn (Friston et al. 2006; Poldrack 2007). As a result, parcellation via functional localizer scans may introduce bias and/or inappropriately constrain the definition of a particular region of interest (Friston et al., 2006). Moreover, functional localizer scans are of little use in identifying a region of interest when: 1) the response properties of the that area are poorly defined or are highly similar to adjacent brain areas; or 2) the response properties of the region of interest are atypical (e.g., areas of deafferented sensory cortex). With these shortcomings in mind, there has been a renewed interest in examining markers that allow individual brain regions to be identified based on structural differences.

Myeloarchitecture

There has been significant interest in myelin - a lipid-protein sheath that envelops axons of the central and peripheral nervous system - as a potential anatomical basis for cortical parcellation (e.g., Nieuwenhuys 2013). Within the central nervous system, myelin density is highest in white matter, with myelinated fibers extending into gray matter throughout the cortex (Vogt 1903). Generally, the density of myelinated fibers decreases from deep to superficial cortical layers; however, the absolute density of myelin across cortical depth can be highly heterogeneous across regions of the brain. These differences arise from local differences in cortical thickness, compactness of fiber layers, and the length and strength of radial fiber bundles (Nieuwenhuys 2013). Moreover, myelin density may differ across regions due to differences in the nature of the computations performed and/or patterns of connectivity to other areas of the brain. For example, myelin density has been shown to be inversely correlated with intracortical circuit complexity (Glasser et al. 2014). Accordingly, myelin gradients have been observed in typically developed sensory cortices, whereby core regions show higher levels of myelination than areas at subsequent steps along the

functional hierarchies to which they project (Glasser and Van Essen 2011; Glasser et al. 2014; Miller et al. 2012; Miller et al. 2013). Since myelination may limit novel synapse formation and/or rearrangement, these hierarchical gradients may contribute to the observation that core sensory regions often show limited evidence of experience-dependent plasticity compared to higher-level regions that appear more responsive to ongoing sensory experience (Glasser et al. 2014; McGee et al. 2005). These myelination gradients are also in accordance with spatiotemporal patterns of development (Brody et al. 1987; Kinney et al. 1988) whereby sensory regions that develop earlier in life are myelinated earlier and more completely than regions that develop at a later age (Miller et al, 2012; Miller et al. 2013; Stadelmann et al. 2019).

Importantly, non-invasive methods have been developed that appear sensitive to the amount of myelin in different brain regions (see Lazari & Lipp 2021 for review). These methods typically involve MR imaging, and take advantage of the fact that myelin content affects relaxation rates (Mackay et al. 2009), magnetization transfer (Wolff & Balaban 1989), and the direction of local diffusion of water molecules within the myelin sheath (Beaulieu 2002). These approaches have historically been limited to estimating the myelin content of cubic mm-sized voxels within the brain; however recent advances in MRI sequences and multi-compartment modeling have improved the spatial resolution of non-invasive myelin quantification (Heath et al. 2018; Mezer et al. 2013). Thus, myelin density is expected to vary in a predictable manner across cortical regions, and these differences may be quantifiable both histologically and via non-invasive approaches across humans and animal models.

Myelin as a biomarker of plasticity/disease

As a result of its role in accelerating action potential propagation, myelin has been shown to be integral in shaping and supporting large-scale functional neural networks (Hunt et al. 2016). Moreover, cortical myelination has been shown to be sensitive to early experience and dynamic across the lifespan, reflecting individual differences in experience, learning, and functional status (Mount and Monje 2017). The onset of complex cognitive processes in humans occurs concurrently with the maturation of myelin-rich regions of the CNS (Williamson and Lyons 2018; Scantlebury et al. 2014; Mabbot et al. 2006). However, periods of social deprivation, particularly early in development, have been associated with a reduction of myelin content in the medial prefrontal cortex (Liu et al. 2012; Makinodan et al. 2012; Long et al. 2018). Additionally, significant changes in myelin density within the intraparietal sulcus have been observed following training on a complex, visually-guided motor skill (Scholz et al. 2009), while impairing the differentiation of oligodendrocytes during task learning significantly impairs retention (Kaller et al. 2017).

Atypical myelination is observed in a number of conditions associated with disrupted cortical function. For example, myelin lesions are commonly associated with Multiple Sclerosis (Rahmanzadeh et al. 2021), while schizophrenia (Takahashi et al. 2011), Amyotrophic Lateral Sclerosis, and Huntington's disease (Huang et al. 2015) show characteristic changes in myeloarchitecture. Moreover, a growing body of literature suggests Alzheimer's disease is associated with atypical patterns of myelination (Ota et al. 2019), and that changes in myeloarchitecture may correlate with the onset of Alzheimer's symptomatology (Maitre et al. 2023). The clear relationships between myeloarchitecture and experience-dependent plasticity/disease etiology underscore the important role that myelin quantification may play in tracking the anatomical status of cortical regions, surgical planning, and in predicting associated functional change following therapeutic interventions.

The present study: Quantifying myelination of auditory cortex

In order to assess the potential of myelin density to parcellate cortical subregions within an established functional hierarchy, the current study sought to quantify patterns of myelination across the auditory

cortex. The feline auditory cortex comprises 13 distinct regions, including two core areas (A1, AAF), three additional low-level regions that are tonotopically organized (PAF, VPAF, VAF), five higher-order regions that respond to more complex acoustic features (A2, fAES, DZ, IN, T) and three multisensory regions that integrate auditory and non-auditory perceptual cues (dPE, iPE, vPE; Lee & Winer, 2011). These regions can be further divided into two parallel streams of processing: a dorsal stream specialized for the representation of auditory space, and a ventral stream specialized in spectral analysis (Lee & Winer 2011). Within each stream, detailed functional hierarchies have been proposed based on patterns of thalamocortical projections to, and corticocortical projections between regions (Lee & Winer 2011; Figure 1). These 'connectional fingerprints' have been effectively used to delineate cortical regions and infer functional hierarchies across a number of species (e.g., macaque: Stephan et al. 2001; human: Behrens & Johansen-Berg 2005), and have been shown to correlate with changes in both cytoarchitecture and function in the feline auditory cortex (Rose & Woolsey 1948). Here, we aim to 1) quantify regional differences in myelin density in feline auditory cortex; and 2) examine the extent to which myelin density is related to the position of a given region within the functional hierarchy of sound processing.

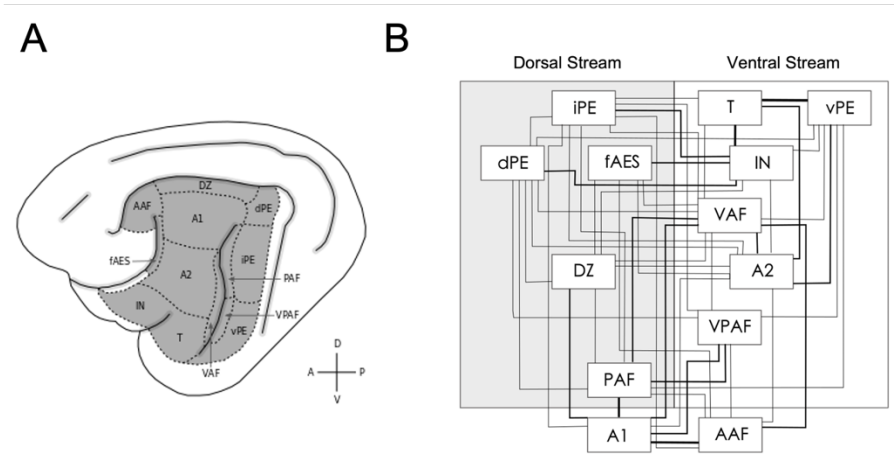

Figure 1. A. Lateral view of the feline brain highlighting auditory cortical regions. B. Hierarchical arrangement of these regions (adapted from Lee & Winer 2011). A1: primary auditory cortex; AAF: anterior auditory field; PAF: posterior auditory field; VPAF: ventral posterior auditory field; DZ: dorsal zone; A2: second auditory cortex; VAF: ventral auditory field; dPE/iPE/vPE: dorsal/intermediate/ventral divisions of posterior ectosylvian gyrus; fAES: auditory division of the anterior ectosylvian sulcus; IN: insular area; T: temporal area.

Methods

Patterns of MFLD were examined in three male domestic short-haired cats obtained from a USDA licensed commercial breeding facility (Marshall Bioresources; Waverly, NY). At the time of sacrifice, each animal was anesthetized with ketamine (4 mg/kg, i.m.) and dexdomitor (0.03 mg/kg, i.m.) and a catheter was inserted into the cephalic vein. Sodium pentobarbital (40 mg/kg, i.v.) was administered to induce general anesthesia, and heparin (1 mL: anticoagulant) and 1% sodium nitrite (1 mL: vasodilator) were administered intravenously. Each animal was then transcardially perfused with physiological saline (1 L), followed by 4% paraformaldehyde (2 L), and 10% sucrose (2L). Following perfusion, brains were blocked in the coronal plane between Horsley-Clarke levels A18 and P2 (a region spanning the entirety of auditory cortex; Horsley & Clarke, 1908), removed, and immersed in a 30% sucrose solution until sunk for cryoprotection (~1 week). Brains were then sectioned in the coronal plane at a thickness of 60 um using a cryostat (Thermo-Fisher, Waltham, Mass). Six series were collected at 360 um intervals: two series were stained for myelin using a modified Gallyas Silver Impregnation method (Gallyas 1979,

Pistorio et al. 2006, Joseph et al. 2019); one series was processed using the monoclonal antibody SMI-32 (Biolegend; Sternberger & Sternberger 1983) to allow for laminar and areal delineation of auditory cortical subfields; one series was stained for Nissl bodies using cresyl violet to assist with delineation; and two series served as spaced to be processed as necessary.

SMI-32 Immunohistochemistry

Antibodies sensitive to SMI-32 recognize a non-phosphorylated epitope of neurofilament proteins, a ligand that is differentially expressed across regions of the auditory cortex, allowing them to be delineated (Mellot et al. 2010). To visualize patterns of SMI-32 reactivity, sections were rinsed with 0.1M physiological buffer (PB; 3 x 5 min), and endogenous peroxidase was blocked with 0.5% hydrogen peroxide in 70% ethanol (30 min). Sections were then rinsed with 0.1 M PB (4 x 5 min), incubated in 5% normal goat serum in 0.1M PB (45 min), and incubated in mouse-anti-SMI-32 antibody (Vector Laboratories, Burlingame, CA, USA; 1/2000 in 2% NGS in 0.1M PB) overnight. The following day, sections were rinsed with 0.1 M PB (4 x 5 min) and incubated in biotinylated goat anti-mouse IgG antibody (Vector Laboratories: 1/200 in 2% NGS in 0.1M PB) for 30 min. Sections were then rinsed with 0.1 M PB (3 x 10 min), and incubated in an avidin–biotin–horseradish peroxidase solution (Vectastain Elite ABC, Vector Laboratories) for 90 minutes. Sections were then rinsed with 0.1 M PB (3 x 10 mins), and incubated with a diaminobenzene–nickel chromogen solution for 15 min. Finally, sections were rinsed with 0.1 M PB (3 x 5 min), mounted from 0.01 M PB on gelatinized slides, air-dried, cleared, and coverslipped.

Myelin Staining

The silver impregnation method (Gallyas 1979; Hackett 2001; Miller et al. 2012, 2013) allows for the visualization of individual myelinated fibers in cortical tissue. To stain for myelin, sections were rinsed in deionized water (3 x 5 min), and then incubated in a 2:1 solution of pyridine and acetic anhydride (30 minutes). Sections were then rinsed in 0.5% acetic acid (3 x 3 min), and incubated in an Ammoniacal Silver solution (0.1% ammonium nitrate, 0.1% silver nitrate w/v; 60 min). Sections were subsequently rinsed in 0.5% acetic acid (3 x 3 min) and incubated in a developer solution containing equal parts sodium carbonate anhydrous (5% w/v), and a solution of ammonium nitrate (0.2% w/v), silver nitrate (0.2% w/v), and tungstosilicic acid hydrate (1% w/v) for 5 minutes. Sections were then rinsed with deionized water (3 x 5 min) and bleached in potassium ferricyanide solution (0.5% w/v; 3 min) before being rinsed again in deionized water (3 x 5 min). This process of development, bleaching, and rinsing was repeated twice to ensure the tissue was well-developed and uniformly stained. At that point, tissue was fixed by incubating in sodium thiosulfate (0.5% w/v; 5 min), and rinsed thoroughly in deionized water (3x10 min). Sections were mounted from gel alcohol (gelatine [1% w/v] in equal parts deionized water and 95% alcohol) on gelatinized slides, air dried, cleared, and coverslipped with permount prior to counting.

Myelin Quantification

Mounted sections were examined using a Zeiss AxioImager M2 microscope equipped with a Lumina HR camera. First, regions of interest (ROIs) throughout auditory cortex were defined for each animal based on patterns of SMI-32 expression (Mellott et al. 2010) using the contour feature in StereoInvestigator (MBF Bioscience; Williston, VT). The 13 regions of the feline auditory cortex were identified, and each was further divided into supragranular (layers I-III), granular (layer IV), and infragranular layers (layers V-VI) for a total of 39 ROIs in each animal. These ROIs were then transferred to adjacent sections stained for myelin to define the boundaries within which myelin estimates were drawn. Myelinated fiber length density (MFLD) was computed as the length of myelinated fiber found within a given volume of tissue, and estimates for each ROI were generated using the Spaceballs probe (Mouton et al. 2002) in StereoInvestigator (MBF Bioscience; Williston, VT) under Koehler illumination at 100x. The Spaceballs

probe has been used extensively to generate unbiased length estimates based on the probability that the surface of a spherical or hemispherical volume of tissue is intersected by a linear feature (e.g., myelinated axon). Sampling parameters for the current study are provided in Table 1, and were selected to ensure that between 70-100 probes would be evaluated within each ROI across a minimum of 3 sections (Schmitz & Hof 2005). Hemispheric Spaceballs probes were placed in a systematic random fashion across each ROI, and the points at which myelinated fibers intersected the surface of the probe were marked. To convert myelin length estimates generated by Stereoinvestigator to length density estimates, the total myelin length obtained for each ROI was divided by the total tissue volume of that ROI. Tissue volumes were estimated by Stereoinvestigator by multiplying the total area of the ROI by the mean mounted thickness which was measured at every 5th sampling location. Finally, the coefficient of error for each estimate was computed to ensure that the variability of the estimate was sufficiently low to ensure an accurate stereological estimate (Schmitz & Hof 2005; see Appendix A).

Statistical Analysis

To allow for comparison across regions of interest of different sizes, myelin length estimates computed for each ROI were divided by the total volume of that ROI to generate myelin length density measures. Myelin length density values were then normalized to an animal's mean MFLD across regions to account for variance that may arise due to differences in the developing/bleaching procedures across animals. Normalized myelin length density values were then compared using a repeated-measures ANOVA with region (13 levels; Figure 1) and depth (infragranular, granular, supragranular) treated as within-subjects factors. Tukey's honestly significant difference test was used to examine differences in myelin density across cortical depths while correcting for multiple comparisons (familywise $\alpha = 0.05$).

To examine how myelin length density varied between regions across the entire thickness of cortex, volume-weighted estimates for each region were computed by multiplying the MFLD observed at each depth by the proportional volume of the ROI at that depth. For example, the myelin density of A1 was computed as follows:

$$MLD_{A1} = \left(MLD_{A1\,supra} \times \frac{Vol_{A1supra}}{Vol_{A1total}}\right) + \left(MLD_{A1gran} \times \frac{Vol_{A1gran}}{Vol_{A1total}}\right) + \left(MLD_{A1infra} \times \frac{Vol_{A1infra}}{Vol_{A1total}}\right)$$

Volume-weighted myelin length density estimates were compared across regions using a repeated-measures ANOVA with region (13 levels) treated as a within-subjects factor. Tukey's honestly significant difference test was used to examine pairwise differences in myelin density while correcting for multiple comparisons.

Results

The current study sought to quantify and compare the patterns of myelination across the feline auditory cortex (Figure 2). Regions of interest were created that comprised the infragranular, granular, and supragranular layers of each of the 13 regions of auditory cortex (for a total of 39 ROIs), and stereological estimates of myelin length density were computed for each ROI. Figure 3 shows the MFLD of each region and cortical depth for each animal examined, as well as the mean MFLD across animals. For ease of visualization, the 13 regions have been arranged according to their position within the proposed functional hierarchy of processing in auditory cortex (Lee & Winer 2011), with dorsal stream regions on the left and ventral stream regions on the right. As expected, significant differences in myelin density were observed across cortical depth ($F(2,4)=111.83$, $p<0.01$); infragranular layers were more densely

myelinated that the granular layer (q=0.354, p<0.001), which was more densely myelinated than the supragranular layers (q=0.616, p<0.001).

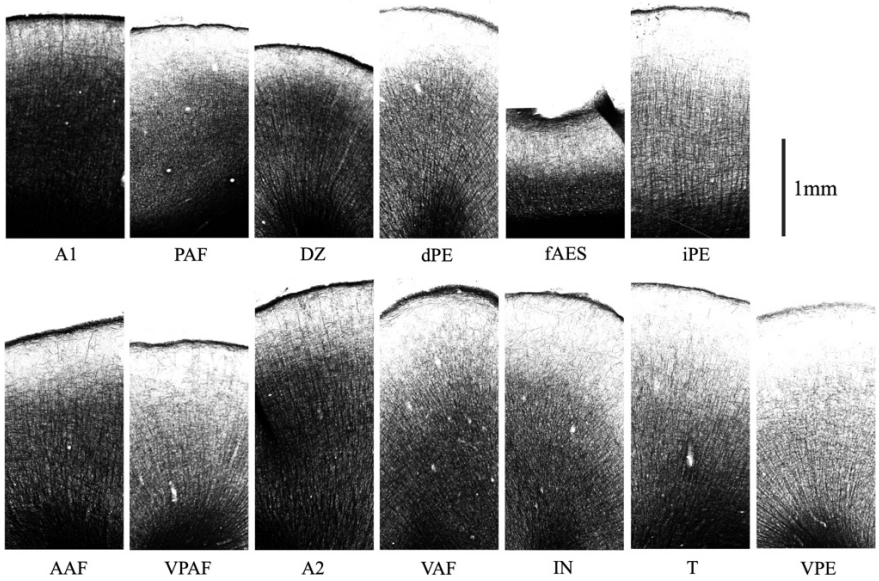

Figure 2. Photomicrographs of cortical myelination across the regions of the feline auditory cortex. Regions are arranged by position within the putative functional hierarchy of processing in auditory cortex (Lee & Winer 2011), with dorsal stream regions on the top, and ventral stream regions on the bottom. Within each image, the cortical surface is positioned at top, with the white matter boundary at bottom. Scale bar shows 1mm.

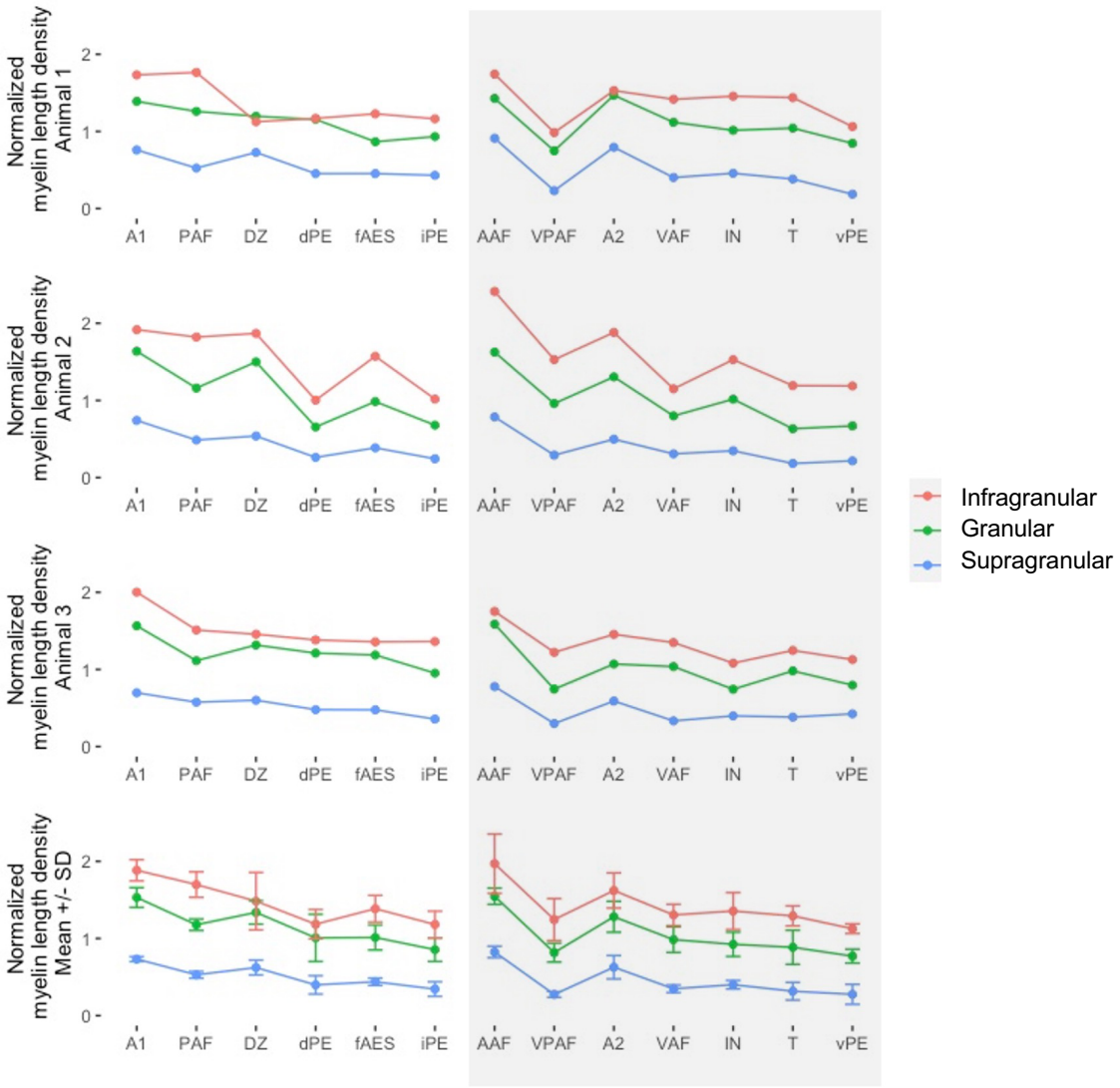

Figure 3. Myelin length density for each auditory cortical region of interest, at each depth examined (red = infragranular, green = granular, blue = supragranular). Regions are arranged by position within the putative functional hierarchy of processing in auditory cortex (Lee & Winer 2011), with dorsal stream regions on the left, and ventral stream regions on the right. Individual animal values (top three panels) were normalized to the mean density across regions within-animal to account for variance that may arise due to differences in the developing/bleaching procedures across animals. A significant depth effect was observed, with myelin density increasing with cortical depth across all regions of interest examined. Error bars in bottom panel show the standard error of the mean.

The effect of depth did not depend on which region of auditory cortex was considered ($F(24,48)=1.18$, $p=0.31$). Accordingly, data were collapsed across depths to examine regional differences in myelin density. To do so, a single volume-weighted estimate of myelin density was computed for each region (Figure 4). A repeated-measures ANOVA using these volume-weighted estimates revealed a significant effect of region ($F(12,24)=12.53$, $p<0.001$). A complete list of pairwise comparisons between regions is provided in Appendix B. In general, myelin density decreased from core to higher level regions within each stream of the putative functional hierarchy. Indeed, differences in myelin density most frequently

reached statistical significance when core regions (primary auditory cortex [A1], anterior auditory field [AAF]) were compared to high level areas (e.g., dorsal, intermediate, and ventral divisions of the posterior ectosylvian gyrus [dPE, iPE, vPE], insular and temporal auditory areas [IN,T], the auditory division of the anterior ectosylvian sulcus [fAES]). Interestingly, despite being placed near the base of the ventral stream functional hierarchy, the ventral posterior auditory field (VPAF) appeared to be less densely myelinated than higher-level areas - an observation that was consistent across animals.

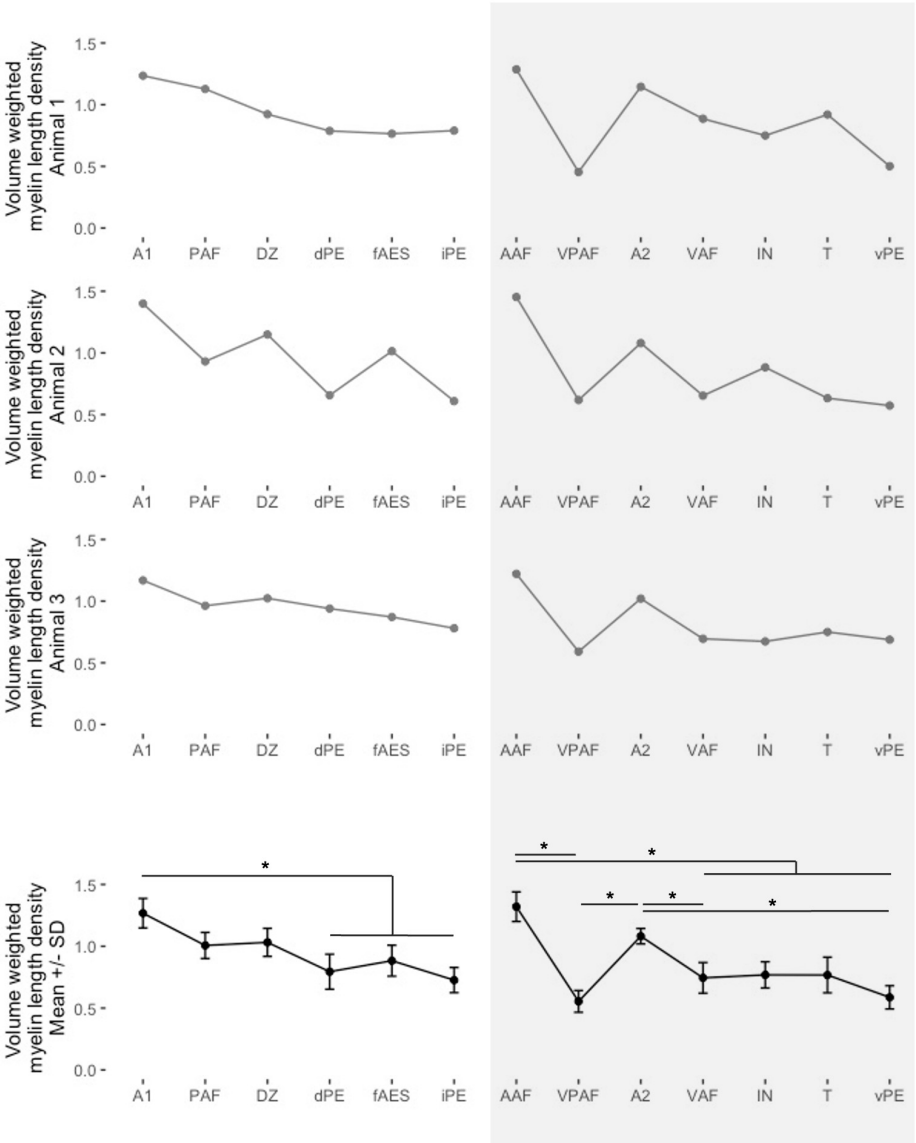

Figure 4. Stereological estimates of myelinated fiber length density (MFLD) for each auditory cortical region of interest. Regions are arranged by position within the putative functional hierarchy of processing in auditory cortex (Lee & Winer 2011), with dorsal stream regions on the left, and ventral stream regions on the right. Error bars in bottom panel show the standard error of the mean. Significant differences in myelin length density within the same stream are shown (* denotes $p < 0.05$, corrected for multiple comparisons [familywise $\alpha = 0.05$]); see appendix A for a summary of all pairwise comparisons.

Discussion

This study presents a detailed quantification and comparison of myelin density across the feline auditory cortex. As expected, MFLD increased with cortical depth across all regions; the deepest layers of cortex, which are most proximal to the white matter, are more densely myelinated than more superficial layers. In human cortex, differences in the relative myelin density between layers occasionally create sharp borders that distinguish adjacent regions (e.g., between divisions of the frontal lobe [Vogt & Vogt 1919]). However, a vast majority of human cortical borders are marked by transitions in myelination that are subtler and more gradual (Von Economo & Koskinas 1925). In the current study, borders between adjacent brain regions were often apparent based on overall myelin density (Figure 2); however, in accordance with previous work in primates (Miller et al. 2013), differences in relative myelin density across depths were nearly uniform across auditory cortex. Thus, myelin density profiles lack the layer-specific differences that have been previously described for other anatomical biomarkers (e.g., SMI-32; Mellott et al. 2010) but are quite effective in parcellating auditory cortex based on overall differences in myelin density.

Regional differences in myelin density

Auditory cortex has been traditionally defined as the portion of the brain that receives its primary thalamic inputs from the dorsal, medial, or ventral divisions of the medial geniculate nucleus (Hackett 2008). Within auditory cortex, distinct regions can be identified based on their patterns of thalamocortical and corticocortical connectivity, differences in anatomical composition, and unique functional properties. Based on these differences, the feline auditory cortex can be segmented into 13 regions (Lee and Winer 2011). In the current study, myelin density varied across these regions in a manner that was highly consistent across animals. Even at low magnification, many of the borders between adjacent regions could be identified based on shifts in myelin density.

The regional differences in myelin density observed here conform to the organizational structure that has been observed across mammalian auditory cortex: one or more ‘core’ regions adjoined by several secondary areas that comprise a ‘belt’, which further project to tertiary regions comprising a ‘parabelt’ (Hackett 2008; Miller et al. 2013). While the core-belt-parabelt structure has been most commonly associated with detailed studies of primate auditory cortex (e.g., Kaas and Hackett 2000), a similar pattern of organization has been proposed based on patterns of corticocortical connectivity observed in the feline brain (Lee and Winer 2008a). It has been previously observed that the regions surrounding the auditory core including A2, DZ, fAES, and PAF show similar, belt-like patterns of thalamocortical (Lee and Winer 2008b) and corticocortical connectivity (Lee and Winer 2008a). Moreover, it was noted that areas along the rostral portion of the posterior ectosylvian gyrus (dPE, iPE, vPE) and at the ventral extent of auditory cortex (In, T) show parabelt-like patterns of projections, with little to no input from core areas (Lee and Winer, 2008a). The current study is in accordance with these connectional data, and suggests that myelin density decreases as one moves from putative core to belt, to parabelt regions of auditory cortex (Figure 5). The existence of a heavily myelinated auditory core is also in accordance with neuroimaging studies of the human auditory cortex (Sigalovsky et al. 2006; Dick et al., 2012; Lutti et al. 2013). Thus, the patterns observed in the current study provide additional support for the feline auditory cortex as a tractable model of the structure and function of human auditory cortex. Moreover, patterns of myelin density may aid in identifying homologous regions across species (Miller et al. 2013), and in aligning cortical maps.

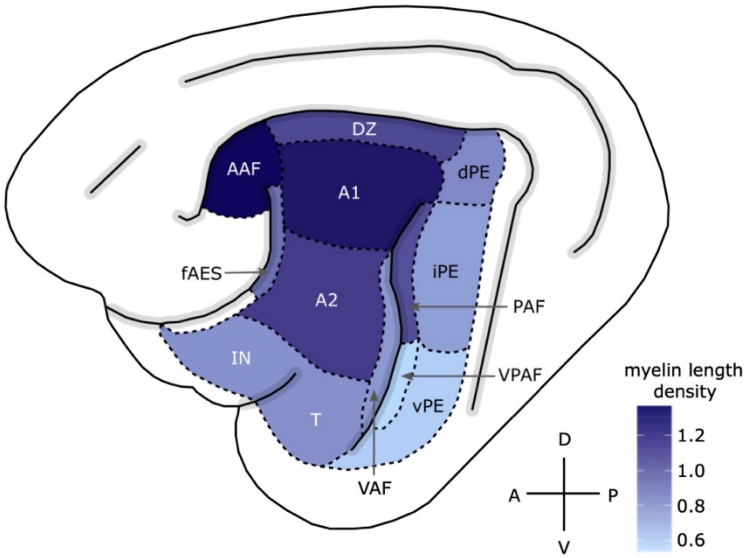

Figure 5. Lateral view of the cat brain showing how myelin length density changes across auditory cortex. Darker colors show regions of denser MFLD (see inset colorbar). AAF: anterior auditory field; fAES: auditory division of the anterior ectosylvian sulcus; DZ: dorsal zone of auditory cortex; A1: primary auditory cortex; A2: second auditory cortex; IN: insular area; T: temporal area; PAF; posterior auditory field; VAF: ventral auditory field; VPAF: ventral posterior auditory field; dPE: dorsal division of the posterior ectosylvian gyrus; iPE: intermediate area of the posterior ectosylvian gyrus; vPE: ventral division of the posterior ectosylvian gyrus.

Hierarchical gradient

The core-belt-parabelt organization of auditory cortex establishes a functional hierarchy wherein ascending thalamocortical projections project predominantly to core regions, which in turn project to higher-level (belt, parabelt) areas. Based on patterns of connectivity, the feline auditory cortex has been further arranged into two parallel functional hierarchies that process information related to sound location (dorsal stream) and spectral composition (ventral stream; Lee & Winer 2011; Figure 1). Based on previous work documenting gradients in myelin density within sensory cortices (e.g., Miller et al. 2013; Dick et al. 2017), the current study predicted that myelin density would decrease with increasing hierarchical position along each of these pathways. Indeed, with the exception of one region (the ventral posterior auditory field; VPAF), the pattern of myelin density observed in the current study conformed to the proposed arrangement.

In part, the hierarchical gradient of myelin density presented here likely reflects regional differences in neuronal density (and thus, differences in the number of myelinated axons per unit volume; see Table 1). However, regional differences may also be related to the time course of neural development, and may play an important role in regional differences in experience-dependent plasticity. As a general principle, myelination ascends along a hierarchical order of increasing functional complexity (Yakovlev & Lecours 1967), and axons in regions that are myelinated early are also myelinated more rapidly and more completely (Stadelmann et al. 2019). Since core regions of auditory cortex are the principal targets of thalamocortical afferents that form the earliest cortical circuitry (Yakovlev & Lecours 1967; Taymourtash et al. 2023), it stands to reason they would be most densely myelinated.

Table 1. Average number of pyramidal somata per 500 um in auditory cortex (from Mellott et al. 2010).

	A1	PAF	DZ	fAES	AAF	VPAF	A2	VAF	IN	T
Layer II	26.3	18.2	34.7	27.3	38.2	0.0	28.7	27.5	0.0	0.0
Layer III	40.7	32.6	58.7	36.8	54.4	0.0	38.6	33.6	0.0	0.0
Layer V	38.1	35.7	48.2	32.8	54.8	19.7	49.5	30.2	29.2	22.8
Layer VI	38.6	15.6	38.6	15.9	34.5	0.0	31.5	23.5	11.4	0.0

*Regions along the posterior ectosylvian gyrus (dPE/iPE/vPE) were not examined in this study
**No somata were counted in layers I/IV

The early development and dense myelination of core auditory cortical areas relative to higher-level regions may contribute to differences in neuroplastic potential across the functional hierarchy. For example, there is evidence that the dorsal zone (DZ; Lomber et al. 2010), posterior auditory field (PAF; Lomber et al. 2010), and auditory field of the anterior ectosylvian sulcus (fAES; Meredith et al. 2011) take on visual functions following profound, early-onset hearing loss; however, evidence for functional reorganization of core feline auditory regions remains contested (Stewart and Starr 1970; Rebillard et al. 1977; Kral et al. 2003). The lack of robust evidence for reorganization in core auditory areas may be related to their myelin density, which has been suggested to play a role in stabilizing existing intracortical circuits by inhibiting the growth of axons and formation of new synapses (Chen et al. 2000; Kapfhammer and Schwab 1994; Glasser et al. 2014). Accordingly, higher-level areas that are more sparsely myelinated may also retain a greater ability to adapt to novel experiences.

Myelin as a marker for non-invasive segmentation

Regional differences in myelin density follow a predictable hierarchy, and many of the borders between regions are readily identifiable based on their relative myelination. Accordingly, the current study supports the idea that myelin density may be an effective biomarker for segmenting functionally distinct auditory cortical areas. Fortunately, non-invasive means of quantifying myelin have received tremendous attention over the past decade. For example, magnetic resonance imaging-based approaches that purport to be sensitive to myelin include T1w/T2w imaging, myelin water fraction imaging, and various indices based on magnetization transfer imaging (e.g., magnetization transfer ratio, magnetization transfer saturation) and diffusion imaging, among others (see Lazari and Lipp 2021 for review). MRI-based approaches to quantifying myelin rely upon proxy measures (e.g., differential rates of relaxation, inferences drawn from the spin properties or motion of water molecules). While many of these measures have been shown to correlate with histological estimates, methodological variance across studies and evidence of publication bias have obscured direct comparisons across approaches (Lazari and Lipp 2021). By quantifying myelin density across auditory cortex, the current study provides detailed histological estimates to which different, less invasive methods can be compared and validated.

Conclusion

Advances in noninvasive quantification of neuroanatomical features has renewed interests in generating detailed histological maps. Myeloarchitectonic maps are of particular interest, as differences in myelin density have been observed within and between cortical regions, and are associated with functional status. Moreover, changes in myelination have been associated with developmental trajectories, patterns of experience, and a number of neurological disorders. The current study provides detailed qualifications of

myelin density across the feline auditory cortex - 13 functionally distinct regions that form two parallel hierarchies of processing. Regional differences in myelination are in line with the classical core-belt-parabelt organization of auditory cortex, and reveal a hierarchical pattern in which lower-level regions are more densely myelinated than higher-order areas. The results presented here provide important insights into the anatomical organization of auditory cortex, and confirm that quantifiable differences in myelin density between brain regions are reliably observed. Moreover, these detailed histological quantifications provide ground-truth estimates against which other, less invasive measures of myelin density may be compared. Overall, the current study highlights the potential of myelin density as a biomarker for cortical parcellation, and for the study of how the anatomy and physiology of specific brain regions are affected by individual experience.

References

Annese J (2009) In Retrospect: Brodmann's brain map. Nature 461:884 https://doi.org/10.1038/461884a

Beaulieu C (2002) The basis of anisotropic water diffusion in the nervous system – a technical review. NMR Biomed 15:435–455. https://doi.org/10.1002/nbm.782.

Behrens TE, Johansen-Berg H (2005) Relating connectional architecture to grey matter function using diffusion imaging. Philos Trans R Soc Lond B Biol Sci 360:903–911. https://doi.org/10.1098/rstb.2005.1640

Brodmann K (1909) Vergleichende Lokalisationslehre der Grosshirnrinde in ihren Prinzipien dargestellt auf Grund des Zellenbaues. Barth, Leipzig, Germany.

Chen MS, Huber AB, van der Haar ME, Frank M, Schnell L, Spillmann AA, Christ F, Schwab ME (2000) Nogo-A is a myelin-associated neurite outgrowth inhibitor and an antigen for monoclonal antibody IN-1. Nature 403:434-9. https:doi.org/10.1038/35000219

Dick FK, Lehet MI, Callaghan MF, Keller TA, Sereno MI, Holt LL (2017) Extensive Tonotopic Mapping across Auditory Cortex Is Recapitulated by Spectrally Directed Attention and Systematically Related to Cortical Myeloarchitecture. J Neurosci. 37:12187-12201. https://doi.org/10.1523/JNEUROSCI.1436-17.2017.

Dick F, Tierney AT, Lutti A, Josephs O, Sereno MI, Weiskaupf N (2012) In vivo functional and myeloarchitectonic mapping of human primary auditory areas. J Neurosci 32:16095-16015. https://doi.org/10.1523/JNEUROSCI.1712-12.2012.

Friston KJ, Rotshtein P, Geng, JJ, Sterzer P, Henson RN (2006) A critique of functional localisers. NeuroImage 30:1077–1087. https://doi.org/10.1016/j.neuroimage.2005.08.012

Gallyas F (1979) Silver staining of myelin by means of physical development. Neurol Res. 1:203-209. https://doi.org/10.1080/01616412.1979.11739553

Glasser MF, Van Essen DC (2011) Mapping human cortical areas in vivo based on myelin content as revealed by T1- and T2-weighted MRI. J Neurosci 31:11597–11616. https://doi.org/10.1523/JNEUROSCI.2180-11.2011

Glasser MF, Goyal MS, Preuss TM, Raichle ME, Van Essen DC (2014). Trends and properties of human cerebral cortex: correlations with cortical myelin content. Neuroimage 93:165-175. https://doi.org/10.1016/j.neuroimage.2013.03.060

Hackett TA, Preuss TM, Kaas JH (2001) Architectonic identification of the core region in auditory cortex of macaques, chimpanzees, and humans. J Comp Neurol. 441:197-222. https://doi.org/10.1002/cne.1407.

Hackett TA (2008) Anatomical organization of the auditory cortex. Journal of the American Academy of Audiology 19:774-779. https://doi.org/10.3766/jaaa.19.10.5

Heath F, Hurley SA, Johansen-Berg H, Sampaio-Baptista C (2018) Advances in noninvasive myelin imaging. Dev Neurobiol. 78:136-151. https://doi.org/10.1002/dneu.22552.

Huang B, Wei W, Wang G, Gaertig MA, Feng Y, Wang W, et al. (2015). Mutant huntingtin downregulates myelin regulatory factor-mediated myelin gene expression and affects mature oligodendrocytes. Neuron 85:1212–1226. https://doi.org/10.1016/j.neuron.2015.02.027

Hunt BA, Tewarie PK, Mougin OE, Grades N, Jones DKm Singh KD, Morris PG, Gowland PA, Brookes MJ (2016) Relationships between cortical myeloarchitecture and electrophysiological networks. Proceedings of the National Academy of Sciences 113:13510-515. https://doi.org/10.1073/pnas.1608587113.

Joseph S, Werner HB, Stegmüller J (2019) Gallyas Silver Impregnation of Myelinated Nerve Fibers. Bio Protoc. 9. https://doi.org/10.21769/BioProtoc.3436

Kaas JH, Hackett TA (2000) Subdivisions of auditory cortex and processing streams in primates. Proc Natl Acad Sci U S A 97:11793-9. https://doi.org/10.1073/pnas.97.22.11793

Kaller MS, Lazari A, Blanco-Duque C, Sampaio-Baptista C, Johansen-Berg H (2017) Myelin plasticity and behaviour-connecting the dots. Current opinion in neurobiology 47:86–92. https://doi.org/10.1016/j.conb.2017.09.014

Kapfhammer JP, Schwab ME (1994) Increased expression of the growth-associated protein GAP-43 in the myelin-free rat spinal cord. Eur. J. Neurosci. 6:403–411. https://doi.org/10.1111/j.1460-9568.1994.tb00283.x

Kral A, Schroder JH, Klinke R, Engel AK (2003) Absence of cross-modal reorganization in the primary auditory cortex of congenitally deaf cats, Exp Brain Res 153:605-613. https://doi.org/10.1007/s00221-003-1609-z

Lazari A, Lipp I (2021) Can MRI measure myelin? Systematic review, qualitative assessment, and meta-analysis of studies validating microstructural imaging with myelin histology. Neuroimage 230:117744. https://doi.org/10.1016/j.neuroimage.2021.117744.

Lee CC, Winer JA (2008a) Connections of cat auditory cortex: III. Corticocortical system. The Journal of comparative neurology, 507:1920-1943. https://doi.org/10.1002/cne.21613

Lee CC, Winer JA (2008b) Connections of cat auditory cortex: I. Thalamocortical system. The Journal of comparative neurology 507:1879–1900. https://doi.org/10.1002/cne.21611

Lee CC, Winer JA (2011) Convergence of thalamic and cortical pathways in cat auditory cortex. Hear Res. 274:85-94. https://doi.org/10.1016/j.heares.2010.05.008

Liu Y, Lee MK, James MM, Price DL, Borchelt DR, Troncoso JC, et al. (2011). Passive (amyloid-β) immunotherapy attenuates monoaminergic axonal degeneration in the AβPPswe/PS1dE9 mice. J. Alzheimers Dis. 23:271–279. https://doi.org/10.3233/JAD-2010-101602

Lomber SG, Meredith MA, Kral A (2010) Cross-modal plasticity in specific auditory cortices underlies visual compensations in the deaf. Nat Neurosci 13:1421-1427. https://doi.org/10.1038/nn.2653

Long P, Wan G, Roberts MT, Corfas G (2018) Myelin development, plasticity, and pathology in the auditory system. Dev Neurobiol 78:80-92. https://doi.org/10.1002/dneu.22538.

Lutti A, Dick F, Sereno MI, Weiskopf N (2013) Using high-resolution quantitative mapping of R1 as an index of cortical myelination. Neuroimage 93:176-88. https://doi.org/10.1016/j.neuroimage.2013.06.005

Mabbott DJ, Noseworthy M, Bouffet E, Laughlin S, Rockel C (2006) White matter growth as a mechanism of cognitive development in children. Neuroimage 33:936–946. https://doi.org/10.1016/j.neuroimage.2006.07.024

MacKay AL, Vavasour IM, Rauscher A (2009) MR relaxation in multiple sclerosis. Neuroimaging Clin. N. Am 19:1–26. https://doi.org/10.1016/j.nic.2008.09.007

Maitre M, Jeltsch-David H, Okechukwu NG et al. (2023) Myelin in Alzheimer's disease: culprit or bystander?. acta neuropathol commun 11. https://doi.org/10.1186/s40478-023-01554-5

Makinodan M, Rosen KM, Ito S, Corfas G (2012) A critical period for social experience-dependent oligodendrocyte maturation and myelination. Science 337:1357-60. https://doi.org/10.1126/science.1220845.

Mellott JG, Van der Gucht E, Lee CC, Carrasco A, Winer JA, Lomber SG (2010) Areas of cat auditory cortex as defined by neurofilament proteins expressing SMI-32. Hear Res. 267:119-36. https://doi.org/10.1016/j.heares.2010.04.003

Meredith MA, Kryklywy J, McMillan AJ, Malhotra S, Lum-Tai R, Lomber SG (2011) Crossmodal reorganization in the early deaf switches sensory, but not behavioral roles of auditory cortex. Proceedings of the National Academy of Sciences of the United States of America 108:8856-8861. https://doi.org/10.1073/pnas.1018519108

Mezer A, Yeatman JD, Stikov N, Kay KN, Cho NJ, Dougherty RF, Perry ML, Parvizi J, Hua le H, Butts-Pauly K, Wandell BA (2013) Quantifying the local tissue volume and composition in individual brains with magnetic resonance imaging. Nat Med 19:1667-72. https://doi.org/10.1038/nm.3390.

Miller DJ, Duka T, Stimpson CD, Schapiro SJ, Baze WB, McArthur MJ, Fobbs AJ, Sousa AM, Sestan N, Wildman DE, Lipovich L, Kuzawa CW, Hof PR, Sherwood CC (2012). Prolonged myelination in human neocortical evolution. Proceedings of the National Academy of Sciences of the United States of America 109:16480–16485. https://doi.org/10.1073/pnas.1117943109

Miller DJ, Lackey EP, Hackett TA, Kaas JH (2013) Development of myelination and cholinergic innervation in the central auditory system of a prosimian primate (*Otolemu garnetti)*. J. Comparative Neurology 521:3804-3816. https://doi.org/10.1002/cne.23379

Mount CW, MonjeM (2017) Wrapped to Adapt: Experience-Dependent Myelination. Neuron 95:743–756. https://doi.org/10.1016/j.neuron.2017.07.009

Mouton PR, Gokhale AM, Ward NL, West MJ (2002). Stereological length estimation using spherical probes. J. Microsc. 206:54–64. https://doi.org/10.1046/j.1365-2818.2002.01006.x

Nieuwenhuys JR (2013) The myeloarchitectonic studies on the human cerebral cortex of the Vogt-Vogt school, and their significance for the interpretation of functional neuroimaging data. Brain Struct. Funct. 218:303–352. https://doi.org/10.1007/s00429-012-0460-z

Olfert ED, Cross BM, McWilliam AA (1993) Guide to the care and use of experimental animals 2nd edition [Cats]. Canadian council on Animal Care 1.

https://citeseerx.ist.psu.edu/document?repid=rep1&type=pdf&doi=05dd439010d8fc815a068939431aaa8612bccdf6

Ota M, Sato N, Kimura Y, Shigemoto Y, Kunugi H, Matsuda H (2019) Changes of Myelin Organization in Patients with Alzheimer's Disease Shown by q-Space Myelin Map Imaging. Dement Geriatr Cogn Dis Extra. 9:24-33. https://doi.org/10.1159/000493937.

Pistorio AL, Hendry SH and Wang X (2006) A modified technique for high-resolution staining of myelin. J Neurosci Methods 153:135-146. https://doi.org/10.1016/j.jneumeth.2005.10.014

Poldrack RA (2007) Region of interest analysis for fMRI. Social cognitive and affective neuroscience 2:67–70. https://doi.org/10.1093/scan/nsm006

Rahmanzadeh R, Lu PJ, Barakovic M, Weigel M, Maggi P, Nguyen TD, Schiavi S, Daducci A, La Rosa F, Schaedelin S, Absinta M, Reich DS, Sati P, Wang Y, Bach Cuadra M, Radue EW, Kuhle J, Kappos L, Granziera C (2021) Myelin and axon pathology in multiple sclerosis assessed by myelin water and multi-shell diffusion imaging. Brain 144:1684-1696. https://doi.org/10.1093/brain/awab088.

Rebillard G, Carlier E, Rebillard M, Pujol R (1977) Enhancement of visual responses on the primary auditory cortex of the cat after an early destruction of cochlear receptors. Brain Res. 129:162-4. https://doi.org/10.1016/0006-8993(77)90980-5

Rose JE, Woolsey CN (1949) The relations of thalamic connections, cellular structure and evocable electrical activity in the auditory region of the cat. J Comp Neurol 91:441–466. https://doi.org/10.1002/cne.900910306

Scantlebury N, Cunningham T, Dockstader C, Laughlin S, Gaetz W, Rockel C, et al. (2014) Relations between white matter maturation and reaction time in childhood. J. Int. Neurophsychol. Soc. 20:99–112. https://doi.org/10.1017/S1355617713001148

Schmitz C, Hof PR (2005) Design-based stereology in neuroscience. Neuroscience. 130:813-31. https://doi.org/10.1016/j.neuroscience.2004.08.050

Scholz J, Klein MC, Behrens TE, Johansen-Berg H (2009) Training induces changes in white-matter architecture. Nature neuroscience 12:1370–1371. https://doi.org/10.1038/nn.2412

Sigalovsky IS, Fischl B, Melcher JR (2006) Mapping an intrinsic MR property of gray matter in auditory cortex of living humans: a possible marker for primary cortex and hemispheric differences. Neuroimage 32:1524-37. https://doi.org/10.1016/j.neuroimage.2006.05.023.

Stadelmann C, Timmler S, Barrantes-Freer A, Simons M (2019) Myelin in the Central Nervous System: Structure, Function, and Pathology. Physiol Rev 99:1381-1431. https://doi.org/10.1152/physrev.00031.2018.

Stephan KE, Kamper L, Bozkurt A, Burns GA, Young MP, Ko ̈tter R (2001) Advanced database methodology for the Collation of Connectivity data on the Macaque brain (CoCoMac). Philos Trans R Soc Lond B Biol Sci 356:1159–1186. https://doi.org/10.1098/rstb.2001.0908

Sternberger LA, Sternberger NH (1983) Monoclonal antibodies distinguish phosphorylated and nonphosphorylated forms of neurofilaments in situ. Proceedings of the National Academy of Sciences of the United States of America 80:6126-30. https://doi.org/10.1073/pnas.80.19.6126.

Stewart DL, Starr A (1970) Absence of visually influenced cells in auditory cortex of normal and congenitally deaf cats. Exp Neurol 28:525-528. https://doi.org/10.1016/0014-4886(70)90190-1

Takahashi N, Sakurai T, Davis KL, Buxbaum JD (2011) Linking oligodendrocyte and myelin dysfunction to neurocircuitry abnormalities in schizophrenia. Prog Neurobiol. 93:13-24. https://doi.org/10.1016/j.pneurobio.2010.09.004

Taymourtash et al. (2023) Fetal development of functional thalamocortical and cortico–cortical connectivity. Cerebral Cortex 33:5613-24. https://doi.org/10.1093/cercor/bhac446

Tootell RB., Hadjikhani NK, Mendola JD, Marrett S, Dale AM (1998) From retinotopy to recognition: fMRI in human visual cortex. Trends in cognitive sciences 2:174-183. https://doi.org/10.1016/s1364-6613(98)01171-1

Vogt O (1903) Zur anatomischen Gliederung des Cortex cerebri. J Psychol Neurol 2:160–180

Vogt C, Vogt O (1919) Allgemeinere Ergebnisse unserer Hirnforschung. J Psychol Neurol 25:279–468

von Economo CF, Koskinas GN (1925) Die cytoarchitektonik der hirnrinde des erwachsenen menschen. J. Springer.

Williamson JM, Lyons DA (2018) Myelin Dynamics Throughout Life: An Ever-Changing Landscape? Front Cell Neurosci. 12:424. https://doi.org/10.3389/fncel.2018.00424.

Wolff SD, Balaban RS (1989) Magnetization transfer contrast (MTC) and tissue water proton relaxation in vivo. Magn Reson Med 10:135-44. https://doi.org/10.1002/mrm.1910100113.

Yakovlev PI, Lecours AR, Minkowski A, Davis FA (1967) Regional development of the brain in early life.

Zilles K. (2018) Brodmann: a pioneer of human brain mapping - his impact on concepts of cortical organization. Brain 141:3262-3278. https://doi.org/10.1093/brain/awy273

Declarations

Funding: This work received financial support from the Natural Sciences and Engineering Research Council and from BrainsCAN - an initiative funded by the Canada First Research Excellence Fund.

Competing Interests: The authors have no relevant financial or non-financial interests to disclose.

Author Contributions: **Austin Robertson:** Formal Analysis, Investigation, Writing - Original Draft, Visualization. **Daniel J. Miller:** Conceptualization, Methodology, Investigation, Writing - Review & Editing, Supervision. **Adam Hull:** Investigation. **Blake E. Butler:** Conceptualization, Writing - Review & Editing, Supervision, Project Administration, Funding Acquisition.

Data Availability: Data generated during the current study are available on the Open Science Framework.

Ethics Approval: All surgical and experimental procedures were conducted in accordance with the Canadian Council on Animal Care's *Guide to the Care and Use of Experimental Animals* (Olfert et al. 1993) and were approved by the University of Western Ontario Animal Care Committee.

Appendix A. Coefficients of error in myelin length density estimates for each ROI in each animal.

Region	Depth	Animal 1 CoE	Animal 2 CoE	Animal 3 CoE
A1	Infragranular	0.04	0.04	0.05
	Granular	0.05	0.05	0.06
	Supragranular	0.04	0.04	0.05
PAF	Infragranular	0.04	0.05	0.05
	Granular	0.05	0.06	0.05
	Supragranular	0.05	0.05	0.05
DZ	Infragranular	0.05	0.04	0.06
	Granular	0.06	0.06	0.06
	Supragranular	0.05	0.05	0.06
dPE	Infragranular	0.06	0.04	0.05
	Granular	0.06	0.05	0.06
	Supragranular	0.07	0.06	0.05
fAES	Infragranular	0.05	0.06	0.05
	Granular	0.07	0.06	0.05
	Supragranular	0.05	0.05	0.06
iPE	Infragranular	0.05	0.04	0.04
	Granular	0.06	0.06	0.05
	Supragranular	0.06	0.06	0.05
AAF	Infragranular	0.05	0.06	0.05
	Granular	0.06	0.06	0.06
	Supragranular	0.07	0.06	0.05
VPAF	Infragranular	0.05	0.06	0.08
	Granular	0.07	0.07	0.06
	Supragranular	0.09	0.07	0.07
A2	Infragranular	0.05	0.07	0.05
	Granular	0.05	0.06	0.05
	Supragranular	0.05	0.06	0.06
VAF	Infragranular	0.09	0.08	0.07
	Granular	0.08	0.08	0.08
	Supragranular	0.09	0.08	0.06
IN	Infragranular	0.04	0.05	0.05
	Granular	0.05	0.06	0.07
	Supragranular	0.06	0.06	0.06
T	Infragranular	0.04	0.06	0.05
	Granular	0.05	0.08	0.05
	Supragranular	0.06	0.1	0.06
vPE	Infragranular	0.04	0.05	0.06
	Granular	0.06	0.06	0.06
	Supragranular	0.07	0.07	0.06

Appendix B. Full output of Tukey's HSD test showing all pairwise comparisons of weighted myelin length density estimates. * p<0.05; ** p<0.01; ***p<0.001

Region 1	Region 2	q	p	
A1	PAF	-0.261	0.25	
	DZ	-0.236	0.383	
	dPE	-0.473	0.0014	**
	fAES	-0.384	0.0149	*
	iPE	-0.541	0.000218	***
	AAF	0.0525	1	
	VPAF	-0.713	0.0000023	***
	A2	-0.186	0.715	
	VAF	-0.523	0.000359	***
	IN	-0.499	0.00069	***
	T	-0.5	0.000671	***
	vPE	-0.681	0.00000534	***
PAF	DZ	0.0249	1	
	dPE	-0.212	0.538	
	fAES	-0.123	0.975	
	iPE	-0.28	0.171	
	AAF	0.313	0.0842	
	VPAF	-0.452	0.00244	**
	A2	0.0747	1	
	VAF	-0.262	0.245	
	IN	-0.238	0.37	
	T	-0.239	0.364	
	vPE	-0.42	0.00589	**
DZ	dPE	-0.237	0.376	
	fAES	-0.148	0.912	
	iPE	-0.305	0.101	
	AAF	0.289	0.145	
	VPAF	-0.477	0.00124	**
	A2	0.0498	1	
	VAF	-0.287	0.15	
	IN	-0.263	0.24	
	T	-0.264	0.236	
	vPE	-0.445	0.00302	**
dPE	fAES	0.0888	0.998	
	iPE	-0.0681	1	
	AAF	0.526	0.000333	***

	VPAF	-0.24	0.358	
	A2	0.287	0.15	
	VAF	-0.0498	1	
	IN	-0.0259	1	
	T	-0.0269	1	
	vPE	-0.207	0.571	
fAES	iPE	-0.157	0.878	
	AAF	0.437	0.00372	**
	VPAF	-0.329	0.0587	
	A2	0.198	0.634	
	VAF	-0.139	0.943	
	IN	-0.115	0.986	
	T	-0.116	0.985	
	vPE	-0.296	0.123	
iPE	AAF	0.594	0.0000526	***
	VPAF	-0.172	0.801	
	A2	0.355	0.0312	*
	VAF	0.0183	1	
	IN	0.0423	1	
	T	0.0412	1	
	vPE	-0.139	0.941	
AAF	VPAF	-0.766	0.000000616	***
	A2	-0.239	0.367	
	VAF	-0.576	0.0000862	***
	IN	-0.552	0.000165	***
	T	-0.553	0.00016	***
	vPE	-0.733	0.0000014	***
VPAF	A2	0.527	0.000319	***
	VAF	0.19	0.687	
	IN	0.214	0.523	
	T	0.213	0.53	
	vPE	0.0328	1	
A2	VAF	-0.337	0.0488	*
	IN	-0.313	0.0852	
	T	-0.314	0.0833	
	vPE	-0.494	0.000782	***
VAF	IN	0.0239	1	
	T	0.0229	1	
	vPE	-0.158	0.875	

IN	T	-0.00101	1
	vPE	-0.182	0.745
T	vPE	-0.181	0.751